Nano Energy 94 (2022) 106942

Contents lists available at ScienceDirect

Nano Energy

journal homepage: www.elsevier.com/locate/nanoen

Boosting moisture induced electricity generation from graphene oxide through engineering oxygen-based functional groups

Renbo Zhu [a], Yanzhe Zhu [a], Fandi Chen [a], Robert Patterson [a,b], Yingze Zhou [a], Tao Wan [a,*], Long Hu [a,*], Tom Wu [a], Rakesh Joshi [a], Mengyao Li [a,*], Claudio Cazorla [f,*], Yuerui Lu [a,g], Zhaojun Han [a,c,d,e], Dewei Chu [a,*]

[a] School of Materials Science and Engineering, University of New South Wales, Sydney, NSW 2052, Australia
[b] Australian Centre for Advanced Photovoltaics, University of New South Wales, Sydney, NSW 2052, Australia
[c] School of Chemical Engineering, University of New South Wales, Sydney, NSW 2052, Australia
[d] School of Mechanical and Manufacturing Engineering, University of New South Wales, Sydney, NSW 2052, Australia
[e] CSIRO Manufacturing, 36 Bradfield Road, Lindfield, NSW 2070, Australia
[f] Departament de Física, Universitat Politècnica de Catalunya, Campus Nord B4-B5, E-08034 Barcelona, Spain
[g] College of Engineering and Computer Science, Australian National University, Canberra, ACT 2601, Australia

ARTICLE INFO

Keywords:
Graphene oxide
PVA
Acidification
Moisture adsorption
Electricity generation
Functional group

ABSTRACT

Harvesting energy from ubiquitous moisture is attracting growing interest for directly powering electronic devices. However, it is still challenging to fabricate high-performing moisture-electric generators (MEGs) with high and stable electric output. Herein, we report a simple strategy to modify the oxygen-based groups of graphene oxide using hydrochloric acid treatment, which boosts the electric output based on the device structure of graphene oxide/polyvinyl alcohol (GO/PVA) MEGs. The resulting MEG enables a stable voltage of 0.85 V and a current of 9.28 μA (92.8 μA•cm^{-2}), which are among the highest values reported so far. More excitingly, electric output gets further improved by simply assembling four MEG units in series or parallel. Moreover, the MEG shows great commercial potential for flexible and wearable applications. Driven by these advancements, the assembled MEGs can successfully power sensors and calculators. This work opens a new era of advance for a new energy conversion technology able to directly powering electronic devices.

1. Introduction

Harvesting green energy from the environment plays a vital role in the development of wearable and portable electronics. Tremendous efforts have been dedicated to developing various types of generators through thermoelectric [1,2] and photoelectric effects [3,4]. These devices can harvest and then convert the ubiquitous clean energy into easily applicable electricity without harmful pollutants and emissions. However, the construction of these devices generally involves a complex configuration, delicate material preparation and high cost. Recently, moisture-electric generators (MEGs) have attracted rising attention for clean energy harvesting and conversion owing to the abundance of moisture, simple device setup and green chemistry involved [5,6]. It has been estimated that 50% of the absorbed solar energy on earth is consumed for driving water evaporation [7], so it will be highly rewarding if we can harvest this renewable energy using MEG and consequently convert it into electricity.

MEG absorbs water molecules from moisture through oxygen-based chemical bonds and then releases mobilized ions to generate separated charges for electric generation [8,9]. Currently, most high-performing MEGs are fabricated with carbon-based materials, which are environment-friendly and abundant on earth including carbon nanotubes, carbon nanoparticles and graphene oxide (GO). Among them, GO exhibits the most promising potential in achieving high electric generation because of its high specific surface area, abundant oxygen-based groups, and good mechanical properties as well as excellent moisture absorption. Huang et al. used porous GO with a large amount of hydrophilic functional groups for fabricating MEGs, which exhibited great moisture absorption ability and achieved a high voltage of 0.6 V at a relative humidity (RH) of 80% [10]. Additionally, a flexible MEG based

* Corresponding authors.
E-mail addresses: tao.wan@unsw.edu.au (T. Wan), long.hu@unsw.edu.au (L. Hu), mengyao.li1@unsw.edu.au (M. Li), claudio.cazorla@upc.edu (C. Cazorla), d.chu@unsw.edu.au (D. Chu).

https://doi.org/10.1016/j.nanoen.2022.106942
Received 20 September 2021; Received in revised form 27 December 2021; Accepted 8 January 2022
Available online 17 January 2022

on GO material was reported to deliver an open-circuit voltage of 0.7 V and a short-circuit current of 0.22 μA with a small size of 0.8 mm^2, which powered a commercial electronic device by using a simple MEG array [11]. However, it is still challenging to maintain continuously high and stable electric outputs for directly driving the electronic devices. Besides, the voltage or current of MEG is strongly related to the high RH and shows instantaneous output, which inhibit its widespread application in electric generators for long-term operation. Furthermore, the detailed mechanism of electricity generation process should also be investigated for a better understanding and to guide its fabrication and applications in harvesting energy from moisture for powering electronic devices.

In this paper, we present an acidified GO film incorporated with a small amount of polyvinyl alcohol (PVA) for MEG applications. PVA with hydroxyl groups and good viscosity not only absorbs water molecules but also improves the attachment of the film to the substrate, which enhances the device stability and electric output. Consequently, electric output of GO/PVA film is greatly enhanced due to the optimization of functional groups and reduced film resistance after acidification, which provides a facile approach to fabricate MEG with high and steady electric output. The single unit can produce a high voltage of 0.85 V and a remarkable current of 9.28 μA (92.8 μA•cm^{-2}) at a RH of 75%, which are among the highest reported electric outputs of MEGs [6, 12]. The MEG shows a good voltage retention over 2 h (0.85 V for 2 h). Additionally, the detailed mechanism of enhanced electricity output is explained through X-ray photoelectron spectrum (XPS) measurements and density functional theory (DFT) simulations. Moreover, the flexible MEG with the substrate of carbon cloth remains 91% of initial voltage output after 2000 times bending, which shows a great commercial potential for the flexible and wearable applications. More excitingly, by simply assembling four MEG units in series or parallel, the voltage output of 3.38 V or the current output of 40.49 μA is achieved, which is the summation of the output of each unit, respectively. Driven by these achievements, the assembled MEGs can successfully power sensors and calculators. In view of the above realizations, this work opens a new era of advance for a new energy conversion technology able to directly powering electronic devices.

2. Experimental section

2.1. Materials

Hydrochloric acid (HCl), acetic acid, sodium hydroxide (NaOH), polyvinyl alcohol powders (Mw 13000–23000), Ag paste and silver nitrate were purchased from Sigma. GO powders were synthesized by the oxidation of graphite powders according to the Hummers method [13]. 20 mg•mL^{-1} GO dispersion was obtained by dispersing GO powders in distilled water with sonication for 30 min. 20 mg•mL^{-1} PVA solution was obtained by dissolving PVA powders in distilled water with stirring at 90 °C for 30 min

2.2. Fabrication of MEG

The fluorine doped tin oxide (FTO) glass was cut into 1.0 × 2.0 cm^2 pieces and was used as substrate/bottom electrode. FTO glass was then cleaned with ethanol and deionized water, followed by ultraviolet radiation for 30 min. GO dispersion and PVA solution were mixed with a mass ratio of 1:1 (maximum ratio to achieve a good attachment of GO/PVA film onto the substrate) by sonication for 30 min and was then dried directly onto the FTO glass at 50 °C for 12 h to form a 1.0 × 1.0 cm^2 GO/PVA film. The edge of GO/PVA film was covered by the insulative tape to avoid short circuit and Ag paste was printed onto the film as the top electrode. For the films fabricated on the carbon cloth (substrate/bottom electrode), the carbon cloth was soaked in the above GO/PVA dispersion for 30 min and was then dried at 50 °C for 12 h.

2.3. Chemical treatments of MEG

As for MEG acidification, MEG was immersed in HCl solution with different concentrations for 10 min. Then MEG was washed with distilled water until no chloride ion was detected by silver nitrate solution. MEG was then dried at 50 °C for 24 h for electrical measurement and powering electronic devices. As for MEG washed with other reagents, MEG was immersed in the acetic acid or NaOH solution for 10 min and then washed with distilled water until pH= 7.

2.4. Electrical measurement

The electrodes of MEG were connected to a Keysight B2902A precision source/measure unit directly for electric output measurements at room temperature of 25 °C (Fig. S1). The wet N_2 and dry N_2 were used to control RH in the sample chamber. Compressed N_2 was used as dry N_2 to decrease RH in the sample chamber. Wet N_2 was obtained by flowing dry N_2 through the deionized water to increase RH in the sample chamber. For electric output retention measurement, moisture was input by wet N_2 to increase RH and electric output until electric measurement ended. For the measurement of an electric output cycle, moisture was input by wet N_2 to increase RH and electric output until it reached highest value, and then it was eliminated by dry N_2 to decrease RH and electric output. The voltage and current output of multiple units were measured by connecting the units in series and parallel, respectively (Fig. S2).

2.5. Material characterization

X-ray diffraction-Empyrean I was performed for characterizing the films and calculating interlayer spacing by Bragg's law [14]. The elemental compositions were employed by X-ray photoelectron spectroscopy (ESCALAB250Xi spectrometer). The morphological images of GO/PVA films were observed by scanning electron microscopy (FEI Nova NanoSEM 450). Electrochemical impedance spectroscopy (EIS) of MEGs was carried out in a two-electrode system at room humidity (55%) using Autolab PGSTAT302N electrochemical workstation. Kelvin probe force microscopy was adopted to analyse surface potential of GO/PVA films on a Bruker Dimension Icon machine at room humidity (55%).

2.6. First-principles calculations

Density functional theory [15] calculations were performed to theoretically characterize the structural and proton-binding properties of functionalized graphene oxide (i.e., containing epoxy O and OH groups) in the presence and absence of carbon vacancies generated by HCl acidification. The Perdew-Burke-Ernzerhof (PBE) exchange-correlation energy functional [16] was used as it is implemented in the Vienna Ab initio Simulation Package (VASP) software [17], and dispersion long-range interactions were described with the DFT+D3 correction method due to Grimme et al. [18]. The "projector augmented wave" method [19] was employed to represent the ionic cores by considering the following electrons as valence: C 2*s* and 2*s*; O 2*s* and 2*p*; H 1*s*. Wave functions were represented in a plane-wave basis truncated at 650 eV. For integrations within the first Brillouin zone, we employed Monkhorst-Pack k-point grids with a density equivalent to that of a 16 × 16 × 1 mesh for the graphene oxide unit cell by considering a 2.5 nm-thickness vacuum region in the direction perpendicular to the carbon plane. Periodic boundary conditions were applied along the three lattice vectors defining the simulation supercell. Geometry relaxations were performed with a conjugate-gradient algorithm that optimized the ionic positions and shape of the simulation cell. The relaxations were halted when the forces in the atoms were all below 0.01 eV·$Å^{-1}$. By using these technical parameters, total energies were converged to within 0.5 meV per carbon atom. Non-stoichiometric graphene oxide systems were generated by removing one carbon atom out of sixteen graphene oxide unit cells (i.e., 1 out of 32 C atoms).

3. Results and discussions

3.1. Electric output of MEGs

Moisture from water evaporation is an abundant and sustainable resource on the earth (Fig. 1a), which can be harvested by MEG and incorporated into self-powered system. Fig. 1b shows the schematic structure of MEG, where carbon-based materials serve as functional layer, and Ag paste and FTO glass act as top and bottom electrodes, respectively. Moisture from the environment is absorbed by the hydrophilic functional layer, which generates separated charges extracted by top/bottom electrode to achieve electric generation. To optimize the functional layers, three types of materials (GO, PVA and GO/PVA) were used to fabricate the devices, which were tested at RH= 75%. As shown in Fig. S3a—c, the maximum voltage (V_{max}) outputs are 0.48 V for GO, 0.26 mV for PVA and 0.50 V for GO/PVA, respectively. Clearly, GO film (Fig. S3a) outperforms PVA film (Fig. S3b) in generating a high voltage output, but an obvious fluctuation of the voltage was observed. During the electric measurement, GO film could not be tightly attached to FTO glass due to the poor interface adhesion (Fig. S4a), which reduced the stability and reproducibility of voltage output (Fig. S4b). As a contrast, GO/PVA exhibited a high and stable voltage output as the PVA could act as binder to greatly improve the interface adhesion (Fig. S3c). Therefore, GO/PVA is selected as the functional layer to fabricate MEG with a high and stable electric output.

The proton concentration gradient across the functional layer is essential for the proton migration, thus the contribution from this gradient dominates the voltage output. Generally, a higher RH and high protonation levels of the functional layer leads to a larger concentration gradient and higher voltage. Here, we use a HCl solution of different concentrations including 32.0%, 16.0%, 1.0%, 0.5% and 0.0% to treat GO/PVA films and tune the density of its functional groups. As shown in Fig. 1c—d, the corresponding V_{max} of the GO/PVA films are 0.85 V, 0.82 V, 0.69 V, 0.61 V, and 0.50 V, respectively, all of which show no decrease for over 2 h. Moreover, acidified GO/PVA film recovers almost 100% V_{max} after being placed for 1 week (Fig. S5). Notably, the V_{max} of 0.85 V generated by the device treated with 32% HCl is among the highest reported voltages for a single MEG. Clearly, acidification can greatly improve the voltage output because it can enhance the protonation level of the functional layer, leading to a larger protonation gradient. The electric output of MEG acidified by 32.0% HCl in an external sweep voltage is investigated in Fig. S6a. The current output of MEG in positive external voltage is significantly higher than that of MEG in negative external voltage, which results from the difference of MEG

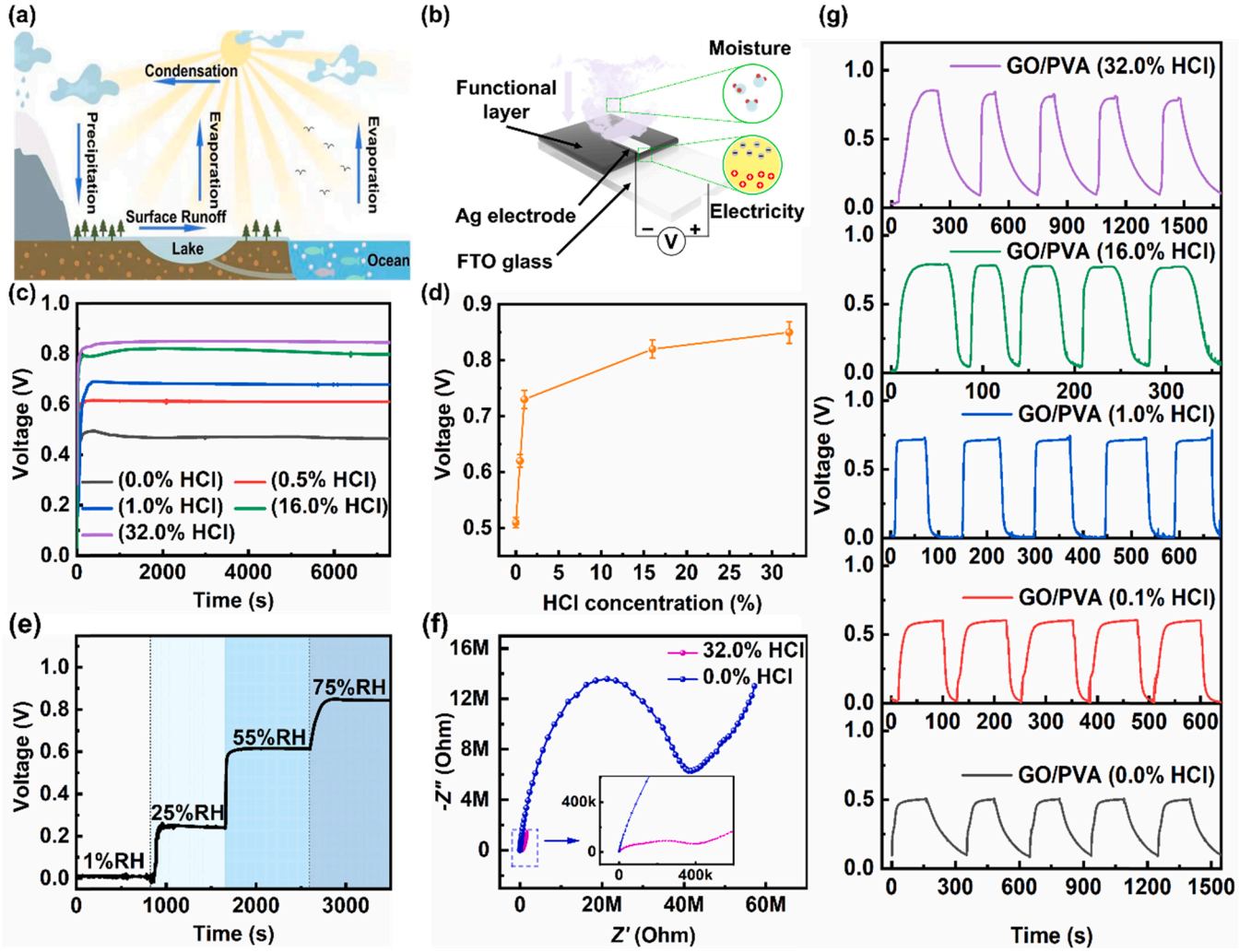

Fig. 1. Electric generation of MEGs. (a) Illustration of abundant and sustainable moisture in the environment. (b) Structure illustration of MEG device. (c) Voltage retention of MEGs acidified with different HCl concentration at RH= 75%. (d) V_{max} of MEGs acidified with different HCl concentration at RH= 75%. (e) Voltage output of MEGs acidified by 32.0% HCl at different RH. (f) EIS of MEGs with and without 32.0% HCl acidification at room humidity of 55%. (g) Voltage output cycle of MEGs acidified with different HCl concentration. In a voltage output cycle, the moisture was input by wet N_2 to increase electric output until it reached highest value and was then eliminated by dry N_2.

resistance. As shown in Fig. S6b, the resistance is 0.02–0.26 MΩ for the positive external voltage and 0.35–2.19 MΩ for the negative external voltage. Therefore, it is indicated that acidified GO/PVA films generate large protonation gradients between top and bottom surfaces. To exclude the effect of residual H^+ after HCl acidification on the improved electric output, the devices were soaked in DI water at a pH of 7 to remove all acid residues. The pH of the final solution was measured using pH indicator sticks (Fig. S7). After soaking the films acidified by 0.0% and 32.0% HCl, respectively, in 1 mL distilled water for 10 min, the pH of the water stabilizes at a pH of 7. Thus, there is some confidence that it is the dissociation of functional groups, rather than contributions from ionized H^+ in the HCl solution, that leads to the protonation gradient.

To exclude variations from other factors, the surface morphology of the GO/PVA films with 0.0% and 32.0% HCl acidification was characterized using scanning electron microscopy (SEM). Fig. S8a—b show that the morphologies of both films are very similar. Cross-sectional SEM images (see Fig. S8c—d) also exhibit that both film microstructure and thickness remain unchanged. Furthermore, the voltage output was measured on devices with different film areas such as 0.5 × 0.5, 1.0 × 1.0 and 1.5 × 1.5 cm^2, exhibiting that voltage remained roughly the same (Fig. S9). Thus, it is possible to achieve high voltage output of MEG with small area. In addition, the V_{max} of PVA films acidified by 32.0% HCl is 0.49 V (Fig. S10), which is much lower than that of GO/PVA films treated with the same conditions. Thus, the acidified GO, instead of acidified PVA, contributes to the high voltage output (V_{max}=0.85 V). Therefore, these results exclude the effects of film morphology, film area and PVA on the high voltage output of the acidified GO/PVA film.

To further confirm that the proton concentration across the films induced the electric potential, devices were exposed to different RH levels (1%, 25%, 55% and 75%). As shown in Fig. 1e, the corresponding V_{max} is 0.02 V, 0.22 V, 0.60 V and 0.85 V. The voltage shows a continuous increase when RH is higher than 75% (Fig. S11). The V_{max} decreases with ambient temperature due to the more water desorption in higher temperature (Fig. S12). Besides, the V_{max} of the acidified film with top/bottom and top/top electrodes at RH= 75% is 0.85 V and 0.02 V, respectively (Fig. S13). MEG with two top electrodes shows almost no voltage output due to negligible protonation gradient between two top sides of GO/PVA films. Thus, protonation gradient is closely related to the voltage output of MEG. Additionally, we investigated the effect of film thickness on the voltage output of GO/PVA films acidified by 32.0% HCl. The GO/PVA films with different thickness of 23.73 μm, 15.33 μm, 12.23 μm and 6.21 μm could produce 0.85 V, 0.85 V, 0.80 V and 0.75 V, respectively (Fig. S14). The MEGs with thinner GO/PVA films facilitate water migration toward inner layer and lead to lower gradient of absorbed water between top and bottom sides, which reduce protonation gradient and voltage output [8,11]. The above results clearly indicate that RH and functional group density in the GO/PVA device co-determine the protonation gradient and voltage output.

Relative humidity is not normally something that can be controlled to produce a high voltage from MEGs in practical applications. Therefore, optimizing functional group density of functional layers is particularly important to obtain desirable voltage and current output. As demonstrated in Fig. 1c, HCl treatments can tune the density of functional groups, which thereby generates various voltage outputs. The cycling stability of the device is another key parameter determining MEG performance. In this work, moisture was carried by N_2 gas to the top surface of the device and the electrical response from the device was measured. When the moisture was extracted by dry N_2, the electric output sharply decreased. The EIS of GO/PVA with and without HCl acidification was carried out in room humidity (RH=55%) to analyse conductivity of different MEGs (Fig. 1f). The GO/PVA with HCl acidification shows a much lower resistance than the GO/PVA without HCl acidification, which is attributed to the more mobile protons in acidified GO/PVA and generates a high current output. Specifically, the maximum current output of the MEG increases from 19.71 nA (197.1 nA•cm^{-2}) to 9.28 μA (92.8 μA•cm^{-2}) after 32.0% HCl acidification (Fig. S15), which is a significant current improvement from the acidification (current increases by 471 times). Fig. 1g shows the voltage cycling of MEGs acidified with different HCl concentration. Clearly, with increasing HCl concentration, the devices produced increased voltages. In each cycle, voltage reaches V_{max} in a short period of 100—250 s with almost 100% voltage recovery efficiency. They demonstrated excellent cycling stability without obvious degradation for each cycle, implying that they may be highly suitable for applications as humidity sensors. To compare device performances achieved in this work, the electrical output of other MEGs recently reported in the literature are summarized in Table 1. Relative to these, our devices exhibit significantly improved electric outputs.

3.2. Working mechanism

The proposed mechanism for power generation from an acidified GO/PVA MEG is illustrated in Fig. 2a, which includes the processes of ionization, charge separation and charge recombination [25]. The protons in the functional groups are immobilized without absorbed water from moisture. During ionization, the moisture on the top side of GO/PVA films facilitates dissociation of functional groups (e.g., –COOH), which releases mobilized H^+ as charge carrier for power generation [8,10,25]. Then, the mobilized H^+ migrates from the top of the device to the bottom since the concentration of mobilized H^+ is higher on the side exposed to the moisture. This leads to charge separation and voltage generation. After moisture removal, the mobilized H^+ migrates back to the top of the device and this leads to charge recombination [11]. Therefore, the charge and discharge processes are triggered by the moisture directly so that MEG can be charged quickly. The device delivers a stable electric output through harvesting the release of clean energy triggered by humidification.

To verify the improved MEG device performance resulting from increased group density after HCl treatment, materials characterization such as X-ray diffraction (XRD), to measure the interlayer spacing in the GO, and XPS measurements, to assess changes in the stoichiometry and bonding, were conducted on the films with and without acidification. The diffraction peaks of GO/PVA film are located at a lower diffraction angle than those of GO films and then gradually shift towards a higher diffraction angle for increased concentrations of HCl in the film treatment (Fig. S16a). The interlayer spacing of GO/PVA film can be calculated by Bragg's law [26,27]. As shown in Fig. S16b, GO/PVA films show

Table 1
Summary and comparison of recent MEGs.

Functional material	Electrode	RH (%)	Output type	Electric output	Refs.
Protein	Au/Au	50	Continuous	0.5 V, 17 μA•cm^{-2}	[8]
TiO_2	Al/ITO	85	Transient	0.5 V, 10 μA•cm^{-2}	[9]
Cellulose paper	Au/ITO	70	Transient	0.25 V, 10 nA•cm^{-2}	[20]
GO	Au/Ag	80	Transient	1.5 V, 27.2 nA•cm^{-2}	[21]
GO/sodium polyacrylate	Au/Ag	80	Continuous	0.6 V, > 1 μA•cm^{-2}	[10]
GO	Au/Au	30	Transient	0.02 V, 5 μA•cm^{-2}	[22]
Cellulosic nanofibrils	Pt/Pt	99	Transient	115 mV, 43 nA•cm^{-2}	[23]
Reduced GO/GO	Au/Au	85	Continuous	0.45 V, 0.9 μA•cm^{-2}	[24]
GO	Au/Au	70	Transient	0.4 V, 2 μA•cm^{-2}	[25]
GO/PVA	Ag/FTO	75	Continuous	0.85 V, 92.8 μA•cm^{-2}	This work

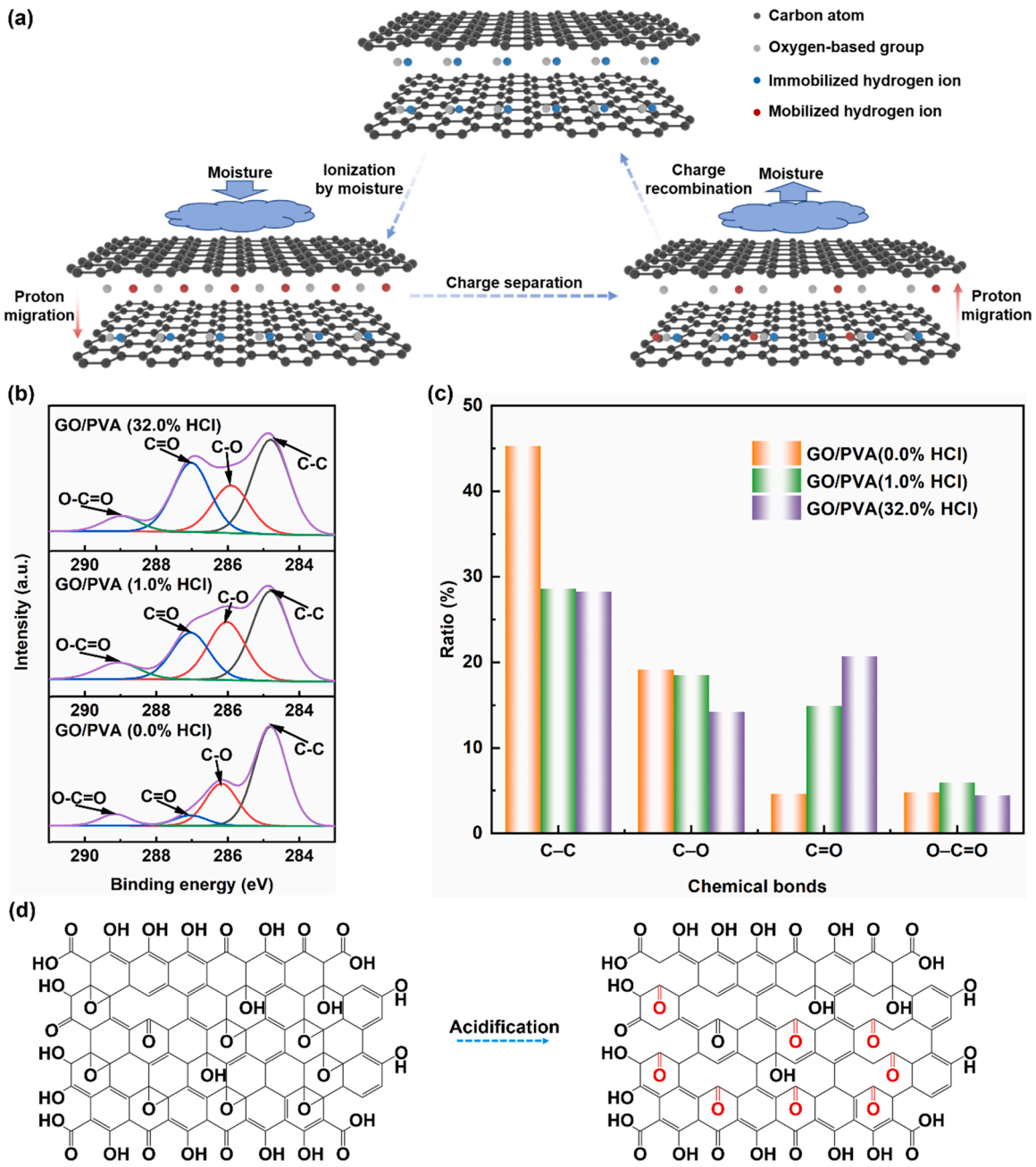

Fig. 2. Characterization and illustration of GO/PVA films in acidification. (a) Electric generation for acidified GO/PVA film. The protons in the functional groups of GO are mobilized by moisture absorption and achieve charge separation by proton migration toward inner layer. Conversely, the migration direction is opposite under the moisture removal and contributes to the charge recombination. (b) XPS spectra of GO/PVA films with and without HCl acidification. (c) The ratio of chemical bonds in the GO/PVA films with and without HCl acidification. (d) Illustration of functional group change in HCl acidification. C—O bonds transform into C═O bonds with better stability after HCl acidification.

a larger interlayer spacing than GO films, where interlayer spacing is 0.77 nm for GO film, 1.26 nm for GO/PVA film (0.0% HCl), 1.19 nm for GO/PVA film (1.0% HCl), and 1.10 nm for GO/PVA film (32.0% HCl). The polymer molecules of PVA can be inserted into the GO interlayer, leading to enlarged interlayer spacing [28,29]. The crosslinking between the GO and PVA bridges the adjacent GO sheets as carboxyl groups from GO can react with hydroxyl groups [30], thus forming a more uniform and stable structure. Besides, the interlayer spacing of GO/PVA films decreased slightly after HCl acidification. The shorten spacing of GO/PVA film with HCl acidification may result from the H^+ introduced in HCl acidification as H^+ can be absorbed by the oxygen-based groups and inhibit the crosslinking of GO and PVA.

Fig. 2b—c show XPS spectra of C 1s region in the GO/PVA films acidified by 0.0% HCl, 1.0% HCl and 32.0% HCl. The C 1 s peaks in the GO/PVA (0.0% HCl) represent the bonds of C–C (45.29 at%), C–O (19.18 at%), C═O (4.67 at%), and O–C═O (4.84 at%). The C 1 s peaks in the GO/PVA (1.0% HCl) represent the bonds of C–C (28.61 at%), C–O (18.50 at%), C═O (14.91 at%), and O–C═O (5.96 at%). The C 1 s peaks in the GO/PVA (32% HCl) represent the bonds of C–C (28.30 at%), C–O (14.26 at%), C═O (20.75 at%), and O–C═O (4.49 at%). Thus, HCl acidification is demonstrated to be a facile approach to tune the density of functional groups. Specifically, the ratio of C–O bonds decreases after HCl acidification, while the ratio of C═O bonds increases after HCl acidification. The GO/PVA films acidified with different HCl concentration present different density of functional groups, which contributes to the performance modification of electricity generation.

It was reported that the film with more C═O bonds exhibits a higher work function and surface potential [31]. The surface potential of GO/PVA films, analysed by Kelvin probe force microscopy (KPFM) under room humidity (RH=55%) in Fig. S17, increases after acidification, which can be ascribed to the increase ratio of C═O bonds.

After HCl acidification, epoxy groups can be arranged in a line, which leads to the rupture of C–C bonds [32,33]. The epoxy chain tends to be oxidized into epoxy pairs and then converted into carbonyl pairs as carbonyl groups are more stable in this condition (Fig. 2d) [34]. The epoxy line and edges are fragile and break up into C═O bonds in HCl acidification. The bonds of C═O with stronger polarity are better than those of C–O for attracting H^+ and forming hydrogen bonds [35]. Based on above analysis, it is proposed that the higher voltage output is attributed to the improved C═O bonds, which attract more H^+ from the dissociation of functional groups, leading to greater protonation gradient for the excellent electric output. Moreover, the carrier (H^+) density in the MEG increases after acidification due to the more dissociated H^+ in the films exposed to the moisture, which leads to the decrease of the film resistance and increase of the current output. To confirm the role of functional groups that contributes to the improvement of voltage output, the oxygen-based groups in the GO/PVA films washed with acetic acid and NaOH were also investigated as shown in Fig. S18. The GO/PVA films washed with acetic acid show the ratio of C–C (35.96 at%), C–O (22.28 at%), C═O (1.27 at%), and O–C═O (6.13 at%), while GO/PVA films washed with NaOH show the ratio of C–C (37.86 at%), C–O (25.24 at%), C═O (2.74 at%), and O–C═O (2.47 at%). The V_{max} of GO/PVA films washed with acetic acid and NaOH is 0.34 V and 0.22 V, respectively, which are much lower than that of the films acidified by HCl as the ratio of C═O in the GO/PVA films washed with acetic acid and NaOH is much lower. Thus, the ratio of C═O is closely related to the electric output of GO/PVA films. Besides, both pristine and acidified GO/PVA films exhibit good hydrophilicity in Fig. S19.

First-principles calculations based on DFT were performed to provide atomistic insights into the observed enhancement effect of electric output induced by HCl acidification of graphene oxide. Specifically, we simulated proton-binding processes for O- and OH-surface functionalized graphene oxide in the presence and absence of carbon vacancies generated by the acidification. Our theoretical DFT results show that the formation of hydrogen bonds between mobile protons and surface immobilized functional groups is significantly increased by the presence of carbon vacancies, a simulation outcome that may explain the enhancement effect of the electrical output observed in the experiments. A summary of our theoretical DFT results is provided in Fig. 3.

In the absence of carbon vacancies (V_C), mobile protons tend to form strong chemical bonds with the O atoms on the carbon surface (Fig. 3a). In this case, the energy corresponding to proton binding amounts to 1.12 eV/H, which leads to H chemisorption and therefore is detrimental for proton migration (i.e., the interactions between O and H turn out to be too strong). Meanwhile, the interactions between mobile protons and surface O atoms become much less intense (i.e., of the order of 0.1 eV) in the presence of V_C defects because the latter are already strongly adsorbed on graphene oxide. Thus, they are not prone to exchange charge with the mobile H^+ ions (Fig. 3b). Consequently, numerous hydrogen bonds involving electrostatic attraction rather fully covalent interactions are formed on the carbon surface, which turns out to be beneficial for proton migration thus achieving higher electric outputs.

In the case of considering functional groups (–OH) on the carbon surface, the general conclusions are very similar to those reported in the paragraph above. It is found that –OH spontaneously detach from the carbon surface upon H binding when V_C are sparse (Fig. 3c). The –OH detachment effect is driven by the formation of water molecules, which relies on charge transfer from the relatively weak C–O surface bonds (i.e., $E_{O\text{-}C} \approx 0.1$ eV) to O–H molecular bonds, and obviously is not desirable for charge-discharge cycling purposes. Conversely, in the presence of abundant carbon vacancies, the –OH that are immobilized near the V_C tend to establish mild hydrogen bonds with the mobile protons (Fig. 3d). In this latter case, it is energetically not favorable to transfer electrons from the very stable C–O surface bonds (i.e., $E_{O\text{-}C} \approx 3.7$ eV) to covalent O–H bonds and thus the mobile H ions are captured by the functional group (–OH) via moderate electrostatic forces.

Overall, our theoretical DFT simulations reproduce the enhancement effect of electric output induced by the type of functional groups that may be introduced by HCl acidification of graphene oxide observed in the experiments. The formation of functional groups to which free protons may form hydrogen bonds may be the underlying cause of the observed improvements.

3.3. Demonstration of application

The MEGs with a high voltage and current output can directly power electronic devices, such as memristors [36] and sensors [37], which significantly improve their practical applications. To further enhance the voltage or current output, MEG units were connected directly in series or parallel (see Fig. S2 for configuration and size of MEG unit). The maximum currents are 9.28 μA, 18.16 μA and 38.95 μA for one unit, two units and four units, respectively (Fig. 4a). In addition, the V_{max} is 0.85 V, 1.70 V and 3.38 V for one unit, two units and four units, respectively (Fig. 4b). Thus, the voltage and current of MEG increase almost linearly with the electric output of one unit (Fig. 4c) and simultaneously remain stable for over 2 h, which demonstrates a great commercial potential for driving electronic devices by simply assembling units in series or parallel. The enhanced electricity generation performance can further widen their applications in areas such as

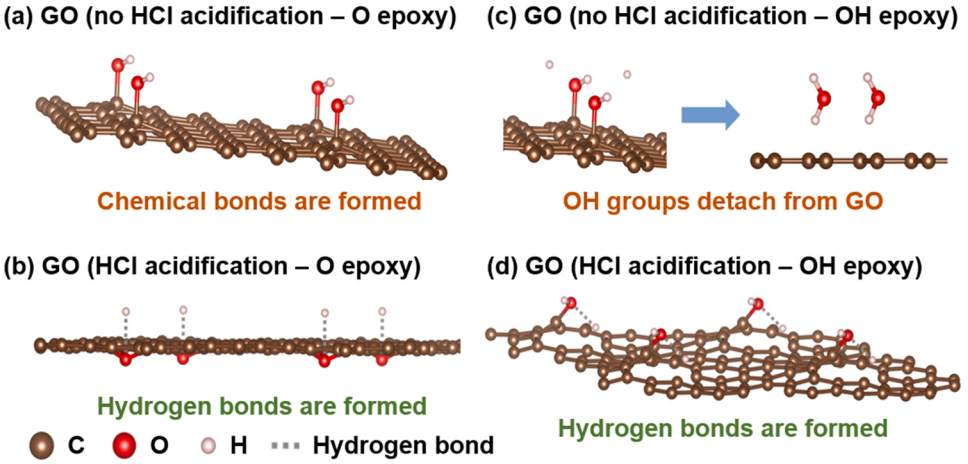

Fig. 3. Theoretical determination of the structural and proton-binding properties of functionalized graphene oxide using DFT calculations. H binding for O-surface functionalized graphene oxide in the absence (a) and presence (b) of carbon vacancies. H binding for OH-surface functionalized graphene oxide in the absence (c) and presence (d) of carbon vacancies. HCl acidification promotes the formation of carbon vacancies. These vacancies lead to functional groups that may hydrogen bond with free protons (~0.1 eV/H) rather than chemically bonding (~1–4 eV/H), leading to high mobility of these protons on hydration.

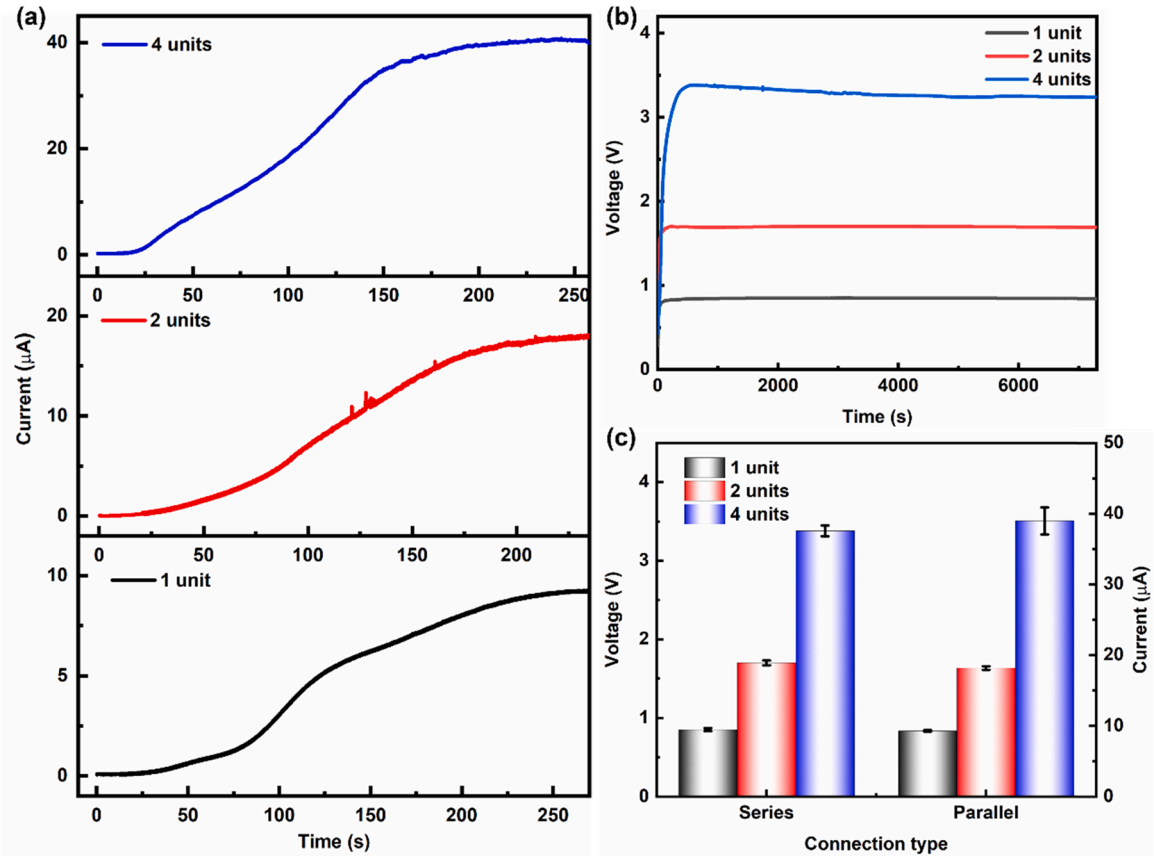

Fig. 4. Electric output of MEGs with different units at RH= 75%. (a) Current output of one unit, two units, four units in parallel. The Ag electrode area of one unit is 0.5 × 0.2 cm^2. (b) Voltage retention of one unit, two units, four units in series. (c) V_{max} and max current output of one unit, two units, four units.

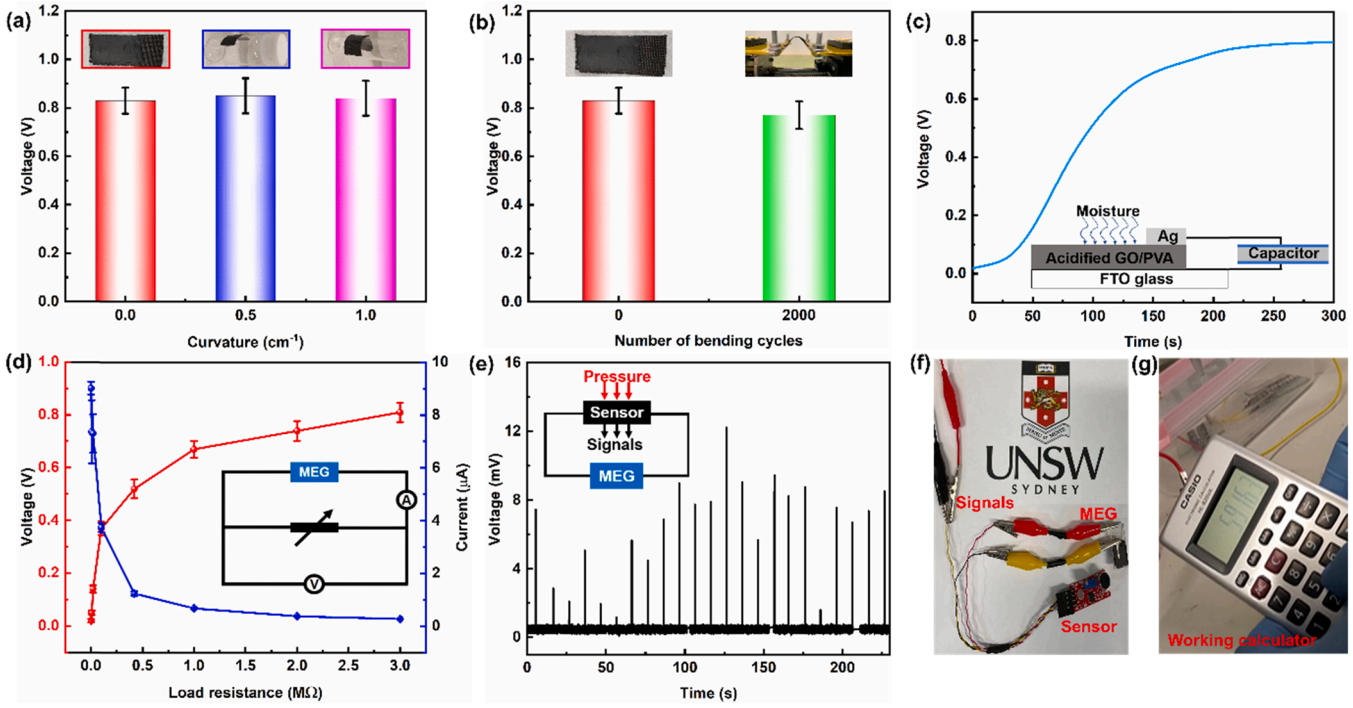

Fig. 5. Demonstration of MEGs as a power source in various practical applications. (a) Voltage output of acidified GO/PVA films wrapped on glass bottle with different curvatures at RH= 75%. (b) V_{max} of acidified GO/PVA on carbon cloth before and after 2000 bending cycles. (c) Voltage output of charging commercial capacitor by MEG at RH= 75%. (d) Electric output of resistor with different resistances connected to MEG at RH= 75%. (e) Voltage signals of pressure sensor powered by MEG at room humidity of 55%. (f) Photograph of commercial pressure sensor powered by a single MEG at room humidity of RH= 55%. (g) Photograph of working calculator powered by MEG with 2 in series × 20 in parallel at RH= 75%.

hydrogen production by catalysis [38,39].

The GO/PVA films with 32.0% HCl acidification are also fabricated on the carbon cloth for flexible device applications. The GO/PVA devices on the carbon cloth are attached to the glass bottles with different radii to investigate the effect of film curvature on the voltage output of GO/PVA films. V_{max} is 0.83 V, 0.85 V and 0.84 V for the films with a curvature of 0.0 cm^{-1}, 0.5 cm^{-1} and 1.0 cm^{-1}, respectively (Fig. 5a). Thus, the GO/PVA devices show stable voltage outputs on the flexible substrates with different curvatures, which demonstrate great potential applications in flexible and wearable electronics. To incorporate GO/PVA film into flexible and wearable application, the film is supposed to show a good electric output in mechanical motion such as bending. The GO/PVA device on the carbon cloth was bent from 0° to 120° in one second. The flexible MEG remained 93% of initial V_{max} after 2000 times bending, which shows a great potential in flexible and wearable applications (Fig. 5b).

Also, MEG demonstrates good stability of charge and discharge cycles (Fig. S20). The MEG can be charged by moisture directly and discharged at a current density of 20 μA•cm^{-2}. The MEG exhibits similar charge/discharge process with good stability for each cycle. The power harvested by MEG from the moisture can also charge the power storage device directly, such as a commercial capacitor (20 μF) charged to 0.80 V in 300 s (Fig. 5c), which exhibits the potential in energy conversion and storage at the same time. The electric output of external device powered by MEG was investigated by connecting loaded resistors with different resistances (Fig. 5d). As load increased from 1 kΩ to 3 MΩ, the voltage of resistor increased from 0.01 V to 0.81 V, whereas the current decreased from 8.55 μA to 0.27 μA. The highest output power across a load resistor was 1.36 μW with a resistance of 0.1 MΩ. Also, a commercial pressure sensor can be powered directly by a single MEG at typical room humidity levels (55%) and generates electric signals according to the external pressure stimulation (Fig. 5e—f and Supplementary Movie S1), which demonstrates a great potential in supplying practical device in room humidity. Moreover, the device array can be easily fabricated by dividing the film into small pieces to supply practical devices as the electric output is unrelated to the film area. The acidified GO/PVA film pattern was fabricated on the FTO glass by the method given above, followed by dividing the films into 20 units in parallel and coating Ag paste on the top sides of all units as the top electrodes (Fig. S21a) to increase its current output. The pattern with 20 units in parallel could also be connected in series to improve the voltage output (Fig. S21b). The arrays (2 in series × 20 in parallel) could provide enough power to supply a commercial calculator (Fig. 5 g and Supplementary Movie S2).

4. Conclusion

In summary, we use HCl-treated GO/PVA to fabricate the MEG because HCl acidification and PVA addition can improve the protonation gradient of MEG and microstructure stability of acidified film on the substrate, respectively, which are beneficial for achieving a high electric output with a good stability. The top surface of acidified GO/PVA film is exposed to moisture directly. While the bottom side is closely sticked to FTO glass, thus robustly blocking moisture penetration. Driven by this moisture asymmetry, the electric output is generated between the top and bottom sides of GO/PVA films. The GO/PVA films, as functional layer, outperform GO films and PVA films by a high and stable voltage output. The voltage output is closely related to the protonation gradient, which can get improved by HCl acidification and high RH. A high voltage of 0.85 V and an excellent current of 9.28 μA (92.8 μA•cm^{-2}) are generated at RH= 75% by GO/PVA films with 32.0% HCl acidification, which can be easily enhanced by connection in series or parallel (3.38 V or 40.49 μA for four units in series or parallel). The voltage of acidified GO/PVA film on flexible carbon cloth shows no obvious decline with film curvatures and bending cycles, which demonstrates a great potential in flexible and wearable application. The acidified GO/PVA films can also be easily divided into pattern for higher electric performance and power a commercial calculator successfully, which is promising in harvesting energy from moisture and powering various practical devices.

CRediT authorship contribution statement

Renbo Zhu: Conceptualization, Data curation, Formal analysis, Investigation, Methodology, Validation, Visualization, Writing – original draft.**Yanzhe Zhu**: Data curation, Formal analysis, Investigation, Methodology. **Fandi Chen**: Data curation, Formal analysis, Investigation, Methodology. **Robert Patterson**: Data curation, Formal analysis, Investigation, Methodology. **Yingze Zhou**: Data curation, Formal analysis, Investigation, Methodology. **Tao Wan**: Data curation, Formal analysis, Investigation, Methodology. **Long Hu**: Data curation, Formal analysis, Investigation, Methodology. **Tom Wu**: Data curation, Formal analysis, Investigation, Methodology, Writing – review & editing. **Rakesh Joshi**: Investigation, Methodology; Writing – review & editing **Mengyao Li**: Data curation, Formal analysis, Investigation, Methodology **Claudio Cazorla**: Software, Validation, Writing – review & editing **Yuerui Lu**: Data curation, Formal analysis, Funding acquisition, Investigation, Methodology. **Zhaojun Han**: Data curation, Formal analysis, Funding acquisition, Investigation, Methodology. **Dewei Chu**: Conceptualization; Data curation; Formal analysis, Funding acquisition, Investigation, Methodology, Project administration, Resources, Supervision, Validation, Visualization, Writing – review & editing.

Declaration of Competing Interest

The authors declare that they have no known competing financial interests or personal relationships that could have appeared to influence the work reported in this paper.

Acknowledgments

The authors would like to acknowledge the financial support from the Australian Research Council Projects (DP210100879, LP190100829). C.C. acknowledges support from the Spanish Ministry of Science, Innovation and Universities under the "Ramon y Cajal" fellowship RYC2018-024947-I. The authors would like to thank Mr. Xiaojun Ren for the assistance in contact angle measurement, and Mr. Yin Yao for the assistance with SEM characterization in Electron Microscope Unit in UNSW.

Appendix A. Supporting information

Supplementary data associated with this article can be found in the online version at doi:10.1016/j.nanoen.2022.106942.

References

[1] J.L. Blackburn, A.J. Ferguson, C. Cho, J.C. Grunlan, Carbon-nanotube-based thermoelectric materials and devices, Adv. Mater. 30 (2018) 1–35, https://doi.org/10.1002/adma.201704386.

[2] D. Zhao, H. Wang, Z.U. Khan, J.C. Chen, R. Gabrielsson, M.P. Jonsson, M. Berggren, X. Crispin, Ionic thermoelectric supercapacitors, Energy Environ. Sci. 9 (2016) 1450–1457, https://doi.org/10.1039/c6ee00121a.

[3] W. Ouyang, F. Teng, J.H. He, X. Fang, Enhancing the photoelectric performance of photodetectors based on metal oxide semiconductors by charge-carrier engineering, Adv. Funct. Mater. 29 (2019) 1–20, https://doi.org/10.1002/adfm.201807672.

[4] S. Park, S.W. Heo, W. Lee, D. Inoue, Z. Jiang, K. Yu, H. Jinno, D. Hashizume, M. Sekino, T. Yokota, K. Fukuda, K. Tajima, T. Someya, Self-powered ultra-flexible electronics via nano-grating-patterned organic photovoltaics, Nature 561 (2018) 516–521, https://doi.org/10.1038/s41586-018-0536-x.

[5] M. Li, L. Zong, W. Yang, X. Li, J. You, X. Wu, Z. Li, C. Li, Biological nanofibrous generator for electricity harvest from moist air flow, Adv. Funct. Mater. 29 (2019) 1–8, https://doi.org/10.1002/adfm.201901798.

[6] J. Bai, Y. Huang, H. Cheng, L. Qu, Moist-electric generation, Nanoscale 11 (2019) 23083–23091, https://doi.org/10.1039/c9nr06113d.

[7] A.H. Cavusoglu, X. Chen, P. Gentine, O. Sahin, Potential for natural evaporation as a reliable renewable energy resource, Nat. Commun. 8 (2017) 617, https://doi.org/10.1038/s41467-017-00581-w.
[8] X. Liu, H. Gao, J.E. Ward, X. Liu, B. Yin, T. Fu, J. Chen, D.R. Lovley, J. Yao, Power generation from ambient humidity using protein nanowires, Nature 578 (2020) 550–554, https://doi.org/10.1038/s41586-020-2010-9.
[9] D. Shen, M. Xiao, G. Zou, L. Liu, W.W. Duley, Y.N. Zhou, Self-powered wearable electronics based on moisture enabled electricity generation, Adv. Mater. 30 (2018) 1–8, https://doi.org/10.1002/adma.201705925.
[10] Y. Huang, H. Cheng, C. Yang, H. Yao, C. Li, L. Qu, All-region-applicable, continuous power supply of graphene oxide composite, Energy Environ. Sci. 12 (2019) 1848–1856, https://doi.org/10.1039/c9ee00838a.
[11] Y. Liang, F. Zhao, Z. Cheng, Y. Deng, Y. Xiao, H. Cheng, P. Zhang, Y. Huang, H. Shao, L. Qu, Electric power generation via asymmetric moisturizing of graphene oxide for flexible, printable and portable electronics, Energy Environ. Sci. 11 (2018) 1730–1735, https://doi.org/10.1039/c8ee00671g.
[12] D. Shen, W.W. Duley, P. Peng, M. Xiao, J. Feng, L. Liu, G. Zou, Y.N. Zhou, Moisture-enabled electricity generation: from physics and materials to self-powered applications, Adv. Mater. 2003722 (2020) 1–31, https://doi.org/10.1002/adma.202003722.
[13] W.S. Hummers, R.E. Offeman, Preparation of graphitic oxide, J. Am. Chem. Soc. 80 (1958) 1339, https://doi.org/10.1021/ja01539a017.
[14] Y. Sheng, X. Tang, E. Peng, J. Xue, Graphene oxide based fluorescent nanocomposites for cellular imaging, J. Mater. Chem. B 1 (2013) 512–521, https://doi.org/10.1039/c2tb00123c.
[15] C. Cazorla, J. Boronat, Simulation and understanding of atomic and molecular quantum crystals, Rev. Mod. Phys. 89 (2017) 1–54, https://doi.org/10.1103/RevModPhys.89.035003.
[16] J.P. Perdew, A. Ruzsinszky, G.I. Csonka, O.A. Vydrov, G.E. Scuseria, L. A. Constantin, X. Zhou, K. Burke, Restoring the density-gradient expansion for exchange in solids and surfaces, Phys. Rev. Lett. 100 (2008) 1–4, https://doi.org/10.1103/PhysRevLett.100.136406.
[17] R.A. Vargas-Hernández, Bayesian Optimization for calibrating and selecting hybrid-density functional models, J. Phys. Chem. A. 124 (2020) 4053–4061, https://doi.org/10.1021/acs.jpca.0c01375.
[18] S. Grimme, J. Antony, S. Ehrlich, H. Krieg, A consistent and accurate ab initio parametrization of density functional dispersion correction (DFT-D) for the 94 elements H-Pu, J. Chem. Phys. 132 (2010), 154104, https://doi.org/10.1063/1.3382344.
[19] P.E. Blöchl, Projector augmented-wave method, Phys. Rev. B 50 (1994) 17953–17979, https://doi.org/10.1103/PhysRevB.50.17953.
[20] X. Gao, T. Xu, C. Shao, Y. Han, B. Lu, Z. Zhang, L. Qu, Electric power generation using paper materials, J. Mater. Chem. A 7 (2019) 20574–20578, https://doi.org/10.1039/c9ta08264f.
[21] Y. Huang, H. Cheng, C. Yang, P. Zhang, Q. Liao, H. Yao, G. Shi, L. Qu, Interface-mediated hygroelectric generator with an output voltage approaching 1.5 volts, Nat. Commun. 9 (2018) 4166, https://doi.org/10.1038/s41467-018-06633-z.
[22] F. Zhao, H. Cheng, Z. Zhang, L. Jiang, L. Qu, Direct power generation from a graphene oxide film under moisture, Adv. Mater. 27 (2015) 4351–4357, https://doi.org/10.1002/adma.201501867.
[23] W. Yang, X. Li, X. Han, W. Zhang, Z. Wang, X. Ma, M. Li, C. Li, Asymmetric ionic aerogel of biologic nanofibrils for harvesting electricity from moisture, Nano Energy 71 (2020), 104610, https://doi.org/10.1016/j.nanoen.2020.104610.
[24] H. Cheng, Y. Huang, F. Zhao, C. Yang, P. Zhang, L. Jiang, G. Shi, L. Qu, Spontaneous power source in ambient air of a well-directionally reduced graphene oxide bulk, Energy Environ. Sci. 11 (2018) 2839–2845, https://doi.org/10.1039/c8ee01502c.
[25] T. Xu, X. Ding, C. Shao, L. Song, T. Lin, X. Gao, J. Xue, Z. Zhang, L. Qu, Electric power generation through the direct interaction of pristine graphene-oxide with water molecules, Small 14 (2018) 1–7, https://doi.org/10.1002/smll.201704473.
[26] T. Xu, X. Ding, Y. Huang, C. Shao, L. Song, X. Gao, Z. Zhang, L. Qu, An efficient polymer moist-electric generator, Energy Environ. Sci. 12 (2019) 972–978, https://doi.org/10.1039/c9ee00252a.
[27] H. Huang, Z. Song, N. Wei, L. Shi, Y. Mao, Y. Ying, L. Sun, Z. Xu, X. Peng, Ultrafast viscous water flow through nanostrand-channelled graphene oxide membranes, Nat. Commun. 4 (2013) 2979, https://doi.org/10.1038/ncomms3979.
[28] R.L.G. Lecaros, G.E.J. Mendoza, W.S. Hung, Q.F. An, A.R. Caparanga, H.A. Tsai, C. C. Hu, K.R. Lee, J.Y. Lai, Tunable interlayer spacing of composite graphene oxide-framework membrane for acetic acid dehydration, Carbon 123 (2017) 660–667, https://doi.org/10.1016/j.carbon.2017.08.019.
[29] R.K. Layek, A.K. Das, M.U. Park, N.H. Kim, J.H. Lee, Layer-structured graphene oxide/polyvinyl alcohol nanocomposites: dramatic enhancement of hydrogen gas barrier properties, J. Mater. Chem. A 2 (2014) 12158–12161, https://doi.org/10.1039/c4ta02346c.
[30] W.S. Hung, Y.H. Chiao, A. Sengupta, Y.W. Lin, S.R. Wickramasinghe, C.C. Hu, H. A. Tsai, K.R. Lee, J.Y. Lai, Tuning the interlayer spacing of forward osmosis membranes based on ultrathin graphene oxide to achieve desired performance, Carbon 142 (2019) 337–345, https://doi.org/10.1016/j.carbon.2018.10.058.
[31] B. Gong, A. Ikematsu, K. Waki, Impacts of structure defects and carboxyl and carbonyl functional groups on the work function of multiwalled carbon nanotubes, Carbon 114 (2017) 526–532, https://doi.org/10.1016/j.carbon.2016.12.046.
[32] D. Pan, J. Zhang, Z. Li, M. Wu, Hydrothermal route for cutting graphene sheets into blue-luminescent graphene quantum dots, Adv. Mater. 22 (2010) 734–738, https://doi.org/10.1002/adma.200902825.
[33] J.L. Li, K.N. Kudin, M.J. McAllister, R.K. Prud'homme, I.A. Aksay, R. Car, Oxygen-driven unzipping of graphitic materials, Phys. Rev. Lett. 96 (2006) 5–8, https://doi.org/10.1103/PhysRevLett.96.176101.
[34] Z. Li, W. Zhang, Y. Luo, J. Yang, J.G. Hou, How graphene is cut upon oxidation? J. Am. Chem. Soc. 131 (2009) 6320–6321, https://doi.org/10.1021/ja8094729.
[35] J.P.M. Lommerse, S.L. Price, R. Taylor, Hydrogen bonding of carbonyl, ether, and ester oxygen atoms with alkanol hydroxyl groups, J. Comput. Chem. 18 (1997) 757–774, https://doi.org/10.1002/(SICI)1096-987X(19970430)18:6<757::AID-JCC3>3.0.CO;2-R.
[36] Y. Tao, Z. Wang, H. Xu, W. Ding, X. Zhao, Y. Lin, Y. Liu, Moisture-powered memristor with interfacial oxygen migration for power-free reading of multiple memory states, Nano Energy 71 (2020), 104628, https://doi.org/10.1016/j.nanoen.2020.104628.
[37] L. Li, Z. Chen, M. Hao, S. Wang, F. Sun, Z. Zhao, T. Zhang, Moisture-driven power generation for multifunctional flexible sensing systems, Nano Lett. 19 (2019) 5544–5552, https://doi.org/10.1021/acs.nanolett.9b02081.
[38] Y. Li, Y. Liu, Q. Qian, G. Wang, G. Zhang, Supramolecular assisted one-pot synthesis of donut-shaped CoP@PNC hybrid nanostructures as multifunctional electrocatalysts for rechargeable Zn-air batteries and self-powered hydrogen production, Energy Storage Mater. 28 (2020) 27–36, https://doi.org/10.1016/j.ensm.2020.02.022.
[39] Q. Shi, Q. Liu, Y. Ma, Z. Fang, Z. Liang, G. Shao, B. Tang, W. Yang, High-performance trifunctional electrocatalysts based on $FeCo/Co_2P$ hybrid nanoparticles for Zinc–Air battery and self-Powered overall water splitting, Adv. Energy Mater. 1903854 (2020) 1–11, https://doi.org/10.1002/aenm.201903854.

Renbo Zhu is currently a PhD candidate under the supervision of Prof. Dewei Chu at the University of New South Wales (UNSW). He received his M.E. degree in Materials Science and Engineering from Central South University in 2019. His research interest focuses on carbon-based materials for moisture-electric generator.

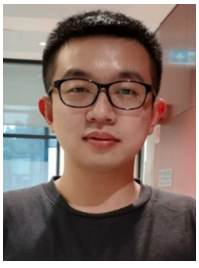

Yanzhe Zhu is a postgraduate student in the School of Materials Science and Engineering, University of New South Wales. He received his bachelor's degree in Northwestern Polytechnical University, and master's degree in University of New South Wales. His research currently focuses on wearable energy storage.

Fandi Chen received his B.E. degree from University of Alabama in 2018 and M.E. degree from University of New South Wales in 2020. He is currently a PhD student under supervision of Prof. Dewei Chu and Prof. Nagarajan Valanoor in MSE school at University of New South Wales. His research interest now lies in resistive switching random access memory.

Robert Patterson is a lecturer in the School of Photovoltaic and Renewable Energy Engineering (SPREE) at the University of New South Wales in Sydney Australia. His research focus has been on chemically synthesized thin film materials and devices as well as colloidal quantum dots for applications in renewable energy, particularly photovoltaic cells.

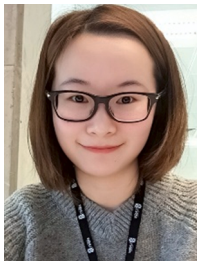

Yingze Zhou is currently pursuing her PhD degree under the supervision of Prof. Dewei Chu at the University of New South Wales (UNSW). She received her M.E. degree in Materials Science and Engineering from the University of New South Wales. Her research interest focuses on precious-metal-free catalysts for electrochemical water splitting and advanced cathode materials for zinc ion batteries.

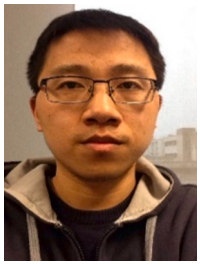

Tao Wan received his PhD degree in the School of Materials Science and Engineering, UNSW Sydney (Australia) in 2018. He is currently a postdoctoral researcher in Prof. Dewei Chu's group. His current research interests include energy harvesting, memory, and optoelectronic devices.

Dr. Long Hu received his PhD degree from Huazhong University of Science and Technology in 2016. He is working as Macquarie Research Fellow at Macquarie University and a visiting fellow at University of New South Wales now. His research interests include nanomaterials synthesis, optoelectronic devices fabrication and energy conversion from sustainable and green source.

Dr. Tom Wu is a Professor of Materials Science and Engineering at UNSW, Sydney. He received his BS degree from Zhejiang University and Ph.D. from the University of Maryland, College Park. He worked at Argonne National Laboratory in Chicago, Nanyang Technological University in Singapore, and KAUST in Saudi Arabia. His research group focuses on exploring novel materials, particularly transition-metal oxides and hybrid halide perovskites, in the form of thin films, nanomaterials and mixed-dimensional heterostructures, targeting at diverse electronic and energy applications, including field-effect transistors, nonvolatile memories, and sensors.

Rakesh Joshi FRSC is an Associate Professor at the School of Materials Science and Engineering, UNSW Sydney, leading the graphene research group. Before joining UNSW, he was a Marie Curie International Fellow at the University of Manchester. He has a PhD in Semiconductor Nanotechnology from the Indian Institute of Technology Delhi. A/Prof. Joshi is among a select group of researchers who have been awarded each of the world's most prestigious relevant International Research Fellowships; the JSPS Invitation Fellowship, the Humboldt Fellowship and the Marie Curie International Fellowship. Rakesh Joshi has over 95 journal articles (and 4 patents), with over 75 articles as the first/corresponding author.

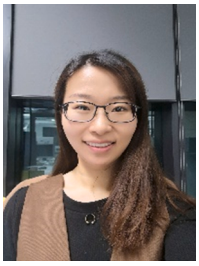

Dr. Mengyao Li's research focuses on sustainable energy such as moist-electric generation and hydrogen evolution generation catalysts of 2D transition metal dichalcogenides. The techniques of optimizing the properties include nanoparticle decoration, phase transformation, element substitution, and single atom intercalation. Currently, Dr. Mengyao Li is working as a postdoctoral research associate in the School of Materials Science and Engineering at UNSW.

Dr. Claudio Cazorla's primary research interests are the application and development of simulation and computational techniques to understand and design materials with potential for energy conversion and energy storage applications. Those techniques include first-principles methods like density functional theory and quantum Monte Carlo and classical molecular dynamics. Currently, Dr. Claudio Cazorla is a "Ramón y Cajal" Fellow at the Department of Physics in the Universitat Politècnica de Catalunya (Barcelona, Spain). Previously, Dr. Claudio Cazorla was awarded several highly prestigious fellowships like the JAE-DOC (Spain) and Australian Research Council Future Fellowship (Australia).

Yuerui Lu is a full Professor at Australian National University (ANU). He received his Ph.D. degree from Cornell University, the school of Electrical and Computer Engineering. He holds a B.S. degree in Applied Physics from University of Science and Technology of China. Currently, he is leading the Nano-Electro-Mechanical System (NEMS) Lab at the ANU. His research interests include MEMS/NEMS sensors and actuators, nanomanufacturing technologies, renewable energy harvesting, biomedical novel devices, and 2D materials and devices.

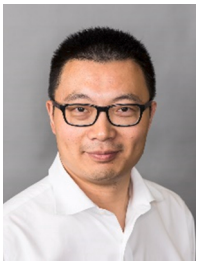

Dr. Zhaojun Han is currently a Senior Research Scientist at Commonwealth Scientific and Industrial Research Organisation (CSIRO) and a Senior Lecturer at the University of New South Wales (UNSW). His research focuses on developing low-dimensional functional materials to tackle the challenges in materials, energy, and environmental science.

Dewei Chu obtained his Ph.D. degree from Shanghai Institute of Ceramics, Chinese Academy of Sciences, China. Then he entered National Institute of Advanced Industrial Science and Technology, Japan as a post-doc researcher. At present, he is a full professor in School of Materials Science and Engineering, University of New South Wales. His research interest focuses on oxide nano materials; nanoelectronics; energy storage materials and devices; functional ceramics, oxide nanocrystals. He published over 160 papers and 7 book chapters.